

UDC 541.67

**THEORETICAL STUDY OF INTERACTIONS BETWEEN
1-ALKYL-3-METHYIMIDAZOLIUM TETRAFLUOROBORATE
AND DIBENZOTHIOPHENE: DFT, NBO, AND AIM ANALYSIS**

M. Niknam¹, M. Vatanparast², H. Shekaari¹

¹*Department of Physical Chemistry, University of Tabriz, Tabriz, Iran*

²*Young Researchers and Elite Club, East Tehran Branch, Islamic Azad University, Tehran, Iran*

E-mail: MVatanparast@yahoo.com (M. Vatanparast)

Received November, 29, 2015

Revised — January, 27, 2016

Density functional theory is employed to study the interaction energies between dibenzothiophene (DBT) and 1-alkyl-3-methylimidazolium tetrafluoroborate ($[C_n\text{mim}]^+[BF_4^-]$). The structures of DBT, 1-ethyl-3-methylimidazolium tetrafluoroborate ($[C_2\text{mim}]^+[BF_4^-]$), 1-butyl-3-methylimidazolium tetrafluoroborate ($[C_4\text{mim}]^+[BF_4^-]$), 1-hexyl-3-methylimidazolium tetrafluoroborate ($[C_6\text{mim}]^+[BF_4^-]$), 1-octyl-3-methylimidazolium tetrafluoroborate ($[C_8\text{mim}]^+[BF_4^-]$), $[C_2\text{mim}]^+[BF_4^-]$ —DBT, $[C_4\text{mim}]^+[BF_4^-]$ —DBT, $[C_6\text{mim}]^+[BF_4^-]$ —DBT and $[C_8\text{mim}]^+[BF_4^-]$ —DBT systems are optimized systematically at the B3LYP/6-31G(*d,p*) level, and the most stable geometries are obtained by NBO and AIM analyses. The results indicate that DBT and imidazolium rings of ionic liquids are parallel to each other. It is found that the $[BF_4^-]$ anion prefers to be located close to a C1—H9 proton ring in the vicinity of the imidazolium ring and the most stable gas-phase structure of $[C_n\text{mim}]^+[BF_4^-]$ has four hydrogen bonds between $[C_n\text{mim}]^+$ and $[BF_4^-]$. There are hydrogen bonding interactions, $\pi-\pi$ and C—H— π interactions between $[C_8\text{mim}]^+[BF_4^-]$ and DBT, which is confirmed by NBO and AIM analyses. The calculated interaction energies for the studied ionic liquids can be used to interpret a better extracting ability of $[C_8\text{mim}]^+[BF_4^-]$ to remove DBT, due to stronger interactions between $[C_8\text{mim}]^+[BF_4^-]$ and DBT, in agreement with the experimental results of dibenzothiophene extraction by $[C_n\text{mim}]^+[BF_4^-]$.

DOI: 10.26902/JSC20170705

К e y w o r d s: dibenzothiophene, desulfurization, ionic liquid, density functional theory, interaction energy.

INTRODUCTION

Sulfur-based components in fuel oil leads to SO_x pollution [1] which has been considered as a main contributing factor to environmental problems. In order to minimize such pollutions strict regulations is being introduced [2] to reduce the sulfur content in fuel oils such as thiophene and its derivatives. The amount of aromatic S-containing compounds in fuel oils depends on the source of crud feedstock, refining methods, the degree of blending [3, 4].

The elimination of aromatic sulfur compounds is difficult due to a lack of appropriate catalysts [5]. Refineries remove organic sulfur from fuel oils by the traditional catalytic hydrodesulfurization (HDS) using catalysts which require both high hydrogen pressure and high temperature [6]. Due to stereochemical barriers, some of the aromatic S-compounds, such as thiophene and its derivatives, have a great resistance to HDS which leads to a costly process that is not affordable to attain the ultralow sulfur fuel [7]. Therefore the oil refineries are increasingly facing technical challenge to effec-

tive removal of trace aromatic S-containing compounds from fuel oils [8] and it is necessary to combine different desulfurization technologies and develop new approaches [9].

Extractive desulfurization of fuel oil under mild conditions is considered as a promising alternative method to the conventional high energy consumption HDS process [10]. In the recent years, the room temperature ionic liquids (ILs) as an innovative alternative for common solvents have been used to extract sulfur containing compounds [11]. They also offer a significant cost reduction and have environmental benefits because of recyclability and non-volatility, in contrast to the volatile organic compounds used nowadays [12]. The room temperature ILs with a low melting point (<100 °C) have unique physical properties such as solubility for a variety of organic/inorganic compounds, good thermal/chemical stability [13], non-flammability [14], recyclability [15], and environmental friendliness [16], which make them suitable extractants for many industrial and laboratory processes. Because of the huge diversity of cation, anion, and alkyl chains, ILs are often referred to designer solvents [12].

The recent literature survey shows that many experimental data have been reported on the extraction of S-containing compounds from fuel oil by different ILs. However, because of numerous ILs, it is hard and very time-consuming in practice to select appropriate IL for such processes.

Therefore, there is need to use theoretical methods as complementary to clarify the nature of solute-solvent interactions in the studied systems and to understand the distinct difference in the extraction performance of IL. To reach this aim, it is necessary to obtain the gas-phase structural information [17] and present interactions between ILs and S-containing aromatic compounds before it can be understood in solution [18].

Many experimental works have been performed on the systems containing IL and model fuel oils to select appropriate IL for the extraction of the aromatic sulfur content [19]. The extraction of thiophene and its derivatives from different model fuel oils with the use of some of these materials was studied, and the experimental results correlated with different thermodynamic models [20—22].

T. Banerjee has studied mixed ILs as possible alternatives for the removal of S-containing aromatics via the conductor like screening model (COSMO) [23] and the selectivity values and the distribution ratio were obtained and compared to single IL. The extraction of thiophene and pyridine from *n*-heptane was investigated using some ILs and the results were modeled by NRTL and UNIQUAC approaches to correlate liquid-liquid equilibrium data [24] and it was found that [Emim]⁺[SCN]⁻ had a good capacity for fuel desulfurization. The results of this work show that [Emim]⁺[SCN]⁻ removes 94 % of thiophene content in model gasoline and 88 % in model diesel oil, while dibenzothiophene is completely extracted from diesel in the third process stage. The infinite dilution activity coefficients of some nitrogen- and sulfur-containing aromatic compounds were predicted via the quantum chemical based conductor like screening model for real solvents (COSMO-RS) model [25]. The results indicate that 4-ethyl-4-methylmorpholium (EMMOR) and 1-ethyl-1-methylpyrrolidinium (EPYRO) gave higher solvent capacity values at infinite dilution of the aromatic nitrogen and sulfur compounds.

Ab initio calculations were carried out for IL mixtures with thiophene and pyridine to investigate the molecular interactions present between IL-thiophene or pyridine. Global scalar properties such as HOMO/LUMO energies, HOMO-LUMO energy gap, chemical hardness, chemical potential, electronegativity, global hardness, global softness, and electrophilicity index were determined for clusters containing ILs with thiophene and pyridine [5]. Based on the results of this work, an overall ranking for the simultaneous removal has the following order: 1-benzyl-3-methyimidazolioum tetrafluoroborate [Bemim][BF₄]⁻ > 1-butyl-3-methylpyrrolidinium tetrafluoroborate [BUMPYR]⁺[BF₄]⁻ > 1-butyl-3-methylpyridinium hexafluorophosphate [BUMPY]⁺[PF₆]⁻ > 1-butyl-3-methylpyridinium tetrafluoroborate [BUMPY]⁺[BF₄]⁻ > 1-butyl-3-methylpyrrolidinium hexafluorophosphate [BUMPYR]⁺[PF₆]⁻. This is in agreement with COSMO-RS predictions.

The interaction between [C₄C₁im]⁺[SCN]⁻ and [C₄C₁im]⁺[NTf₂]⁻ and thiophene was considered by M.L.S. Batista using the molecular dynamics (MD) simulation [26]. Negative excess molar volumes, as well as strong positive chemical shift deviations for the carbon atom in the [SCN]⁻ anion for [C₄C₁im]⁺[SCN]⁻, showed the presence of strong and specific interactions between IL and thiophene protons. These results further supported the MD simulations.

To screen suitable IL, the MD simulations were performed, and DBT along with dibenzothiophene sulfone (DBTO₂) were used as model compounds to study the desulfurization mechanism and the interactions between them and a series of ILs (1-alkyl-3-methylimidazolium cations ($[C_n\text{mim}]^+$, $n = 4, 6, 8, 10$) and $[\text{BF}_4]^-$, $[\text{PF}_6]^-$ anions) [27]. The calculations indicate that DBTO₂ could be extracted by ILs more easily than DBT and the hydrogen bond between O2 and H4 of $[C_{10}\text{mim}]^+[\text{PF}_6]^-$ IL is stronger than that in $[C_{10}\text{mim}]^+[\text{BF}_4]^-$.

Density functional theory has been used to calculate the interaction energy between dibenzothiophene, diphenylsulfide, diphenyldisulfide, benzene, tetralin, and 1-methyl-3-methylimidazolium methyl sulfate ($[\text{Mmim}]^+[\text{MeSO}_4]^-$) [18]. Their results show that there are $\pi-\pi$ interactions between the thiopenic ring and phenyl with the IL imidazolium ring and this type of interaction may be stronger in thiophene than in the phenyl ring due to a higher charge density of aromatic π -electrons in thiophene. The interaction energies between $[\text{Mmim}]^+[\text{MeSO}_4]^-$ and dibenzothiophene are also higher than those in the other compounds studied.

The fundamental nature of the interactions between thiophene and 1-*n*-butyl-3-methylimidazolium hexafluorophosphate ($[C_4\text{mim}]^+[\text{PF}_6]^-$) and 1-*n*-butyl-3-methylimidazolium tetrafluoroborate ($[C_4\text{mim}]^+[\text{BF}_4]^-$) was investigated using *ab initio* calculations and correlated with the previous experimental results [10]. The absorption capacity of thiophene in ILs is strongly dependent on the structure and property of the anion and the compactness between the cation and the anion of ILs. For $[\text{Bmim}]^+[\text{PF}_6]^-$, due to a strong electron donation of the phosphorus atom to fluorine atoms, the fluorine atoms in $[\text{PF}_6]^-$ possess a relatively high negative charge and $[\text{PF}_6]^-$ can also provide more native charged fluorine atoms to thiophene molecules as compared with $[\text{BF}_4]^-$. Moreover, the degree of compactness of $[\text{Bmim}]^+[\text{PF}_6]^-$ is lower than that of $[\text{Bmim}]^+[\text{BF}_4]^-$, which allows a facile restructuring of IL during thiophene dissolution. These differences affect the absorption capabilities of ILs.

In the recent years, it has been found that two kinds of ILs, $[C_n\text{mim}]^+[\text{PF}_6]^-$ and $[C_n\text{mim}]^+[\text{BF}_4]^-$, can effectively absorb a large amount of sulfur-containing aromatic compounds, such as thiophene (TS) and DBT [28]. Data on the interactions between $[\text{Bmim}]^+[\text{BF}_4]^-$ and the DBT system have been obtained by Ren-qing *et al.*, but according to our knowledge, these results have not been investigated systematically by theoretical methods.

Therefore, in this work the quantum chemical calculations were used to investigate the effect of an alkyl chain length of cations in $[C_n\text{mim}]^+[\text{BF}_4]^-$ ILs on the interaction energies with DBT systems at molecular and atomic levels. To achieve this aim, the structures of $[C_2\text{mim}]^+[\text{BF}_4]^-$, $[C_2\text{mim}]^+[\text{BF}_4]^-$ —DBT, $[C_4\text{mim}]^+[\text{BF}_4]^-$, $[C_4\text{mim}]^+[\text{BF}_4]^-$ —DBT, $[C_6\text{mim}]^+[\text{BF}_4]^-$, $[C_6\text{mim}]^+[\text{BF}_4]^-$ —DBT, and $[C_8\text{mim}]^+[\text{BF}_4]^-$, $[C_8\text{mim}]^+[\text{BF}_4]^-$ —DBT complexes, interaction energies, charge populations, and topological properties of the most stable structures were obtained and the geometric parameters were discussed in detail to understand the fundamental interactions between DBT and the four ILs studied.

COMPUTATIONAL METHODS

All geometry and energy optimizations and vibrational frequency and potential energy surface calculations in this work have been carried out using the GAUSSIAN 03W program [29]. The modern density functional theory (DFT) method using the Becke hybrid gradient-corrected (three-parameter nonlocal) exchange functional [30] with the gradient corrected (nonlocal) correlation functional of Lee, Yang, and Parr [31] has been employed for all computations. The geometry optimizations for all possible conformations of the target compounds were performed at the B3LYP/6-31G(*d,p*) level of theory. All the structures in the gas phase have been fully optimized without any geometric constraints. For corroborating the stable structures, the vibrational frequency calculations have been performed, which verify the true minima of the potential energy surface of all structures.

The natural bond orbital (NBO) [32] analysis was carried out at the B3LYP/6-311G++(*d,p*) [30, 31] level of theory using the NBO 3.1 program [33], in order to understand the nature of interactions between the cation, the anion, and DBT. In the NBO analysis, the second order perturbation stabilization energy $E(2)$, kcal/mol⁻¹ associated with the delocalization $i \rightarrow j$ is estimated as

Table 1

Interaction energies of DBT—[C₂mim]⁺[BF₄][−]/[C₄mim]⁺[BF₄][−]/[C₆mim]⁺[BF₄][−] and [C₈mim]⁺[BF₄][−]

Ionic liquids	Interaction energies, kcal/mol ^{−1}	Ionic liquids	Interaction energies, kcal/mol ^{−1}
[C ₂ mim][BF ₄]—DBT	−15.13	[C ₆ mim][BF ₄]—DBT	−17.32
[C ₄ mim][BF ₄]—DBT	−16.16	[C ₈ mim][BF ₄]—DBT	−18.37

$$E(2) = \Delta E_{ij} = n_i \frac{(F_{ij})^2}{\varepsilon_j - \varepsilon_i} \quad (1)$$

where n_i is the donor orbital occupancy, ε_i and ε_j are the diagonal elements, and F_{ij} is the off-diagonal NBO Fock matrix element. The topological properties of the electron density at bond critical points (BCPs) have been characterized using the atoms in molecules methodology (AIM) [34] by means of the AIM2000 software [35] at the B3LYP/6-311++G(*d,p*) level of theory.

The interaction energies are defined as differences between the sum of the DBT and [C₂mim]⁺[BF₄][−]/[C₄mim]⁺[BF₄][−]/[C₆mim]⁺[BF₄][−]/[C₈mim]⁺[BF₄][−] energies and the energies of DBT—[C_nmim]⁺[BF₄][−] (with n : 2, 4, 6, 8) complexes as follows (Table 1):

$$\Delta E = E(\text{Complex}) - [E(\text{DBT}) + E([\text{C}_2\text{mim}]^+[\text{BF}_4]^- / [\text{C}_4\text{mim}]^+[\text{BF}_4]^- / [\text{C}_6\text{mim}]^+[\text{BF}_4]^- / [\text{C}_8\text{mim}]^+[\text{BF}_4]^-)]. \quad (2)$$

RESULTS AND DISCUSSION

Geometric and electronic properties. A number of theoretical studies have been reported concerning the location and orientation of imidazolium-based cations—[BF₄][−] pairs of ILs. The calculated results suggest that [BF₄][−] anions prefer to be located close to a C1-proton ring [36]. The structures of DBT, the [BF₄][−] anion, and [C₂mim]⁺, [C₄mim]⁺, [C₆mim]⁺ and [C₈mim]⁺ cations are shown in Figs. 1 and 2.

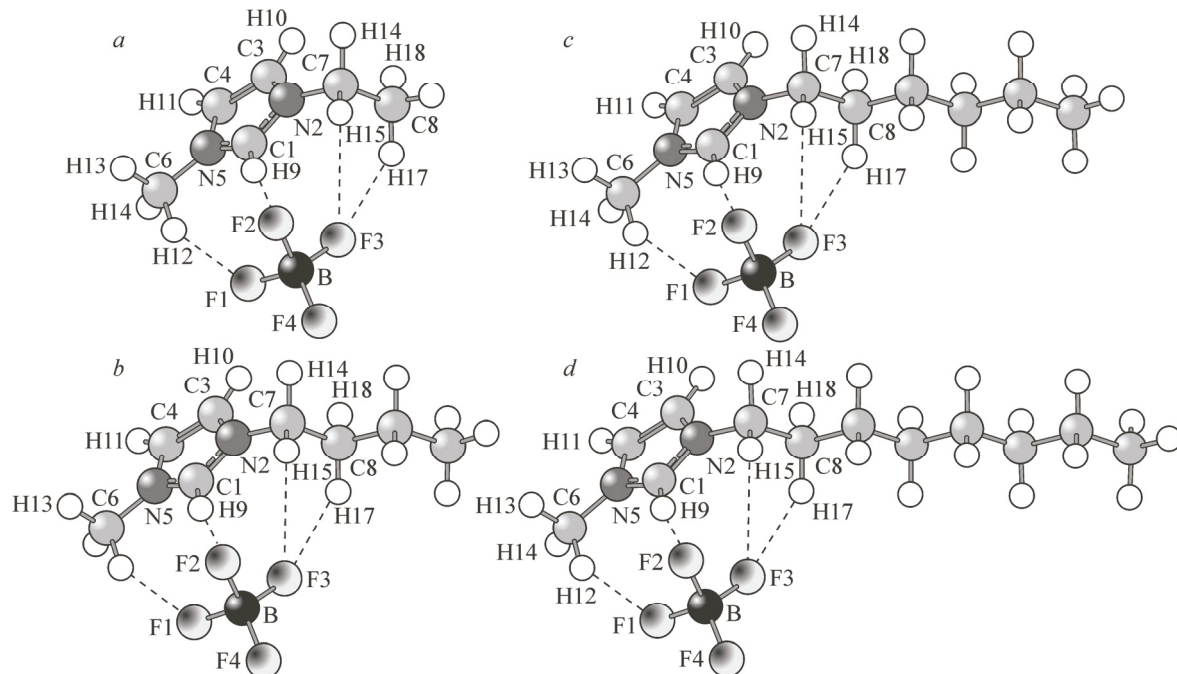


Fig. 1. Optimized structures of: [C₂mim]⁺[BF₄][−] (a), [C₄mim]⁺[BF₄][−] (b), [C₆mim]⁺[BF₄][−] (c), and [C₈mim]⁺[BF₄][−] (d)

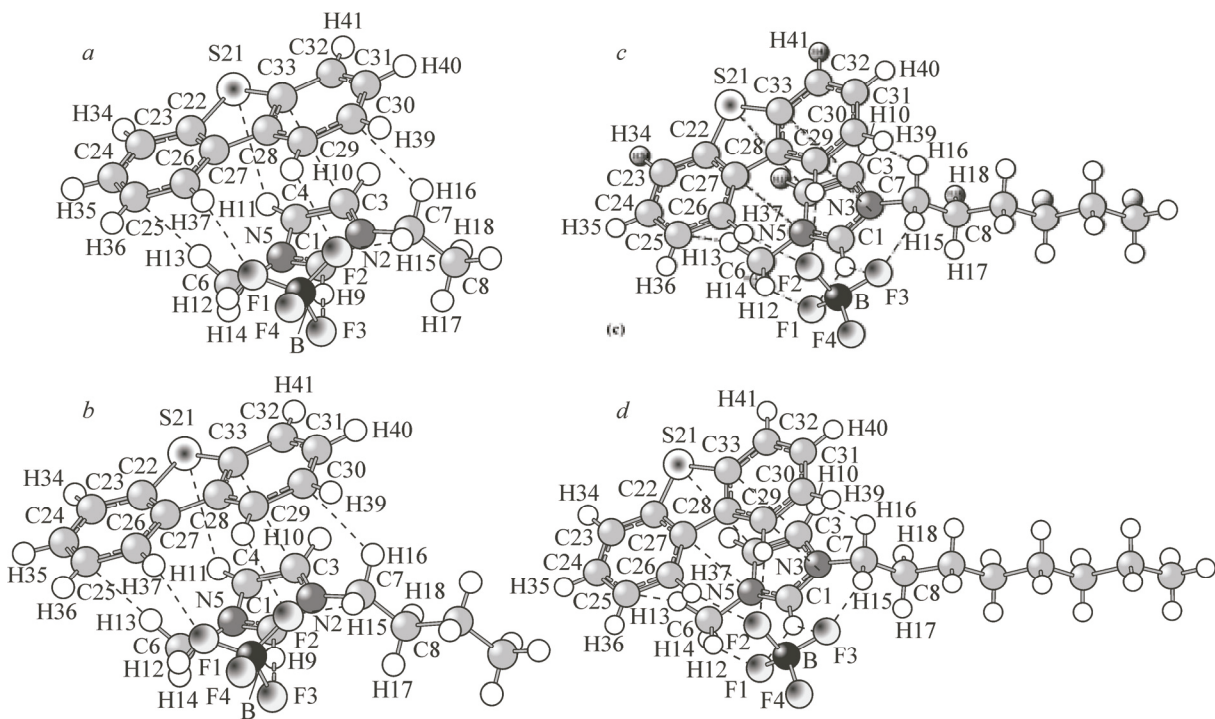


Fig. 2. Optimized structures of: $[C_2\text{mim}]^+[\text{BF}_4]^-$ —DBT (a), $[C_4\text{mim}]^+[\text{BF}_4]^-$ —DBT (b), $[C_6\text{mim}]^+[\text{BF}_4]^-$ —DBT (c), and $[C_8\text{mim}]^+[\text{BF}_4]^-$ —DBT (d)

At the beginning of calculations, the cation and the anion were separately optimized and then the pair of cations and anions was optimized. Finally, in order to optimize the complexes, DBT was placed in different regions around imidazolium-based cations to form $[C_2\text{mim}]^+[\text{BF}_4]^-$ —DBT, $[C_4\text{mim}]^+[\text{BF}_4]^-$ —DBT, $[C_6\text{mim}]^+[\text{BF}_4]^-$ —DBT, and $[C_8\text{mim}]^+[\text{BF}_4]^-$ —DBT.

To examine the structures of $[C_2\text{mim}]^+[\text{BF}_4]^-$, a $[\text{BF}_4]^-$ anion was placed near the corresponding C1—H9, C3—H10, and C4—H11 ring protons in the vicinity of the imidazolium ring. For comparison, $[\text{BF}_4]^-$ anions were placed in the positions around the ethyl chain substituent of the imidazolium ring. The most stable structure of $[C_2\text{mim}]^+[\text{BF}_4]^-$ can be seen in Fig. 1, a. It can be seen that the most stable structure of $[C_2\text{mim}]^+[\text{BF}_4]^-$ has four F···H interactions, corresponding to interacting H15···F3, H17···F3, H9···F2, and H12···F1 distances of 2.874, 2.526, 1.792, and 2.151 Å (Table 2), respectively.

The minimum H9···F2 distance confirms the role of C1—H9 in the formation of the strongest hydrogen bond. Also the hydrogen bonds occur between the fluorine atoms of $[\text{BF}_4]^-$ and C—H of the methyl and ethyl groups (H15, H17, and H12) of the imidazolium ring. It can be seen that a single fluorine atom (F3) participates in two hydrogen bonds. This type of bonding is called the bifurcated hydrogen bonding or the three-centered hydrogen bonding. The initial structures were designed by placing the $[\text{BF}_4]^-$ anion and DBT around the imidazolium ring (two alkyl side chains). The possible π (imidazolium)- π (DBT) interactions were considered with the $[\text{BF}_4]^-$ anion arranged in different positions. Fig. 2, a shows the optimized geometry of $[C_2\text{mim}]^+[\text{BF}_4]^-$ —DBT, in which the interacting distances between $[C_2\text{mim}]^+[\text{BF}_4]^-$ and DBT are 1.806 Å (F3···H9), 2.606 Å (F2···H38), 2.281 Å (F2···H15), 2.485 Å (F1···H37), 2.491 Å (F1···H12), 2.984 Å (C25···H13), 3.343 Å (S21···H11), 3.502 Å (C32···C3), and 3.114 Å (C30···H16). The interacting distances between $[C_2\text{mim}]^+$ and $[\text{BF}_4]^-$ in $[C_2\text{mim}]^+[\text{BF}_4]^-$ —DBT are 1.806 Å (F3···H9), 2.281 Å (F2···H15), and 2.491 Å (F1···H12). The $[C_2\text{mim}]^+$ ring and DBT ring planes are parallel to each other, implying that π — π interactions may occur. The π stacking (also called the π — π stacking) refers to attractive, non-covalent interactions between the aromatic rings.

Table 2

Topological properties of the electron density (ρ , a.u.), the laplacian of density ($\nabla^2\rho$, a.u.), and atomic distances (d , Å) for $[C_2mim]^+[BF_4]^-$, $[C_4mim]^+[BF_4]^-$, $[C_6mim]^+[BF_4]^-$, $[C_8mim]^+[BF_4]^-$, DBT— $[C_2mim]^+[BF_4]^-$ / $[C_4mim]^+[BF_4]^-$ / $[C_6mim]^+[BF_4]^-$ and $[C_8mim]^+[BF_4]^-$, obtained at the B3LYP/6-311++G(d,p) level

Parameter	d	ρ	$\nabla^2\rho$	d	ρ	$\nabla^2\rho$	d	ρ	$\nabla^2\rho$	d	ρ	$\nabla^2\rho$	
		$[C_2mim]^+[BF_4]^-$			$[C_4mim]^+[BF_4]^-$			$[C_8mim]^+[BF_4]^-$			$[C_8mim]^+[BF_4]^-$		
F1···H12	2.151	0.01536	0.05686	2.148	0.01543	0.05720	2.153	0.01529	0.05662	2.160	0.01504	0.05559	
F2···H9	1.792	0.03329	0.12565	1.794	0.03308	0.12485	1.795	0.03301	0.12475	1.794	0.03310	0.12515	
F3···H15	2.874	0.00459	0.02051	2.889	0.00450	0.02029	2.882	0.00457	0.02054	2.876	0.00463	0.02079	
F3···H17	2.526	0.00693	0.02674	2.514	0.00719	0.02739	2.501	0.00739	0.02811	2.488	0.00759	0.02883	
		$[C_2mim]^+[BF_4]^-$ —DBT			$[C_4mim]^+[BF_4]^-$ —DBT			$C_6mim]^+[BF_4]^-$ —DBT			$C_8mim]^+[BF_4]^-$ —DBT		
F1···H9	—	—	—	—	—	—	2.024	0.02024	0.07900	1.975	0.02228	0.08681	
F1···H12	2.491	0.00772	0.02824	2.463	0.00826	0.03012	2.305	0.01071	0.03969	2.406	0.00866	0.03206	
F1···H37	2.485	0.00785	0.02950	2.381	0.00978	0.03675	—	—	—	—	—	—	
F2···H15	2.281	0.01177	0.04139	2.311	0.01112	0.03914	—	—	—	—	—	—	
F2···H37	—	—	—	—	—	—	2.293	0.01104	0.03934	2.295	0.01098	0.03915	
F2···H38	2.606	0.00635	0.02377	2.549	0.00719	0.02664	2.315	0.01065	0.03756	2.313	0.01069	0.03772	
F3···H9	1.806	0.03191	0.12153	1.824	0.03059	0.11638	2.066	0.01880	0.07379	2.122	0.01681	0.06629	
F3···H15	—	—	—	—	—	—	2.272	0.01144	0.04279	2.202	0.01323	0.05020	
S21···C4	—	—	—	—	—	—	3.786	0.00415	0.01285	3.794	0.00409	0.01260	
S21···H11	3.343	0.00404	0.01359	3.329	0.00426	0.01424	—	—	—	—	—	—	
C25···H13	2.984	0.00512	0.01442	2.960	0.00539	0.01526	2.959	0.00547	0.01659	2.982	0.00527	0.01633	
C27···N5	—	—	—	—	—	—	3.551	0.00396	0.01245	3.551	0.00395	0.01247	
C29···N2	—	—	—	3.596	0.00381	0.01139	3.616	0.00382	0.01112	3.606	0.00387	0.01124	
C33···C3	3.502	0.00573	0.01504	3.466	0.00595	0.01567	3.556	0.00503	0.01272	3.578	0.00491	0.01236	
C30···H16	3.114	0.00403	0.01121	2.973	0.00504	0.01376	2.939	0.00547	0.01478	3.105	0.00539	0.01467	

Fig. 1, b shows the final optimized structure of $[C_4mim]^+[BF_4]^-$. The results indicate that it has four F···H interactions, the corresponding interacting H15···F3, H17···F3, H9···F2, and H12···F1 distances being 2.889, 2.514, 1.794, and 2.148 Å, respectively. The shortest H9···F2 distance suggests that C1—H9 is involved in the formation of the strongest hydrogen bond. Hydrogen bonds also occur between the fluorine atoms of $[BF_4]^-$ and C—H of the methyl and ethyl groups (H15, H17, and H12) of the imidazolium ring. The results indicate that a single fluorine atom (F3) participates in two hydrogen bonds. The possible π (imidazolium)- π (DBT) interactions were considered with the $[BF_4]^-$ anion arranged in different positions. The structure optimization result for $[C_4mim]^+[BF_4]^-$ —DBT is shown in Fig. 2, b. In Fig. 2, b, the interacting distances between $[C_4mim]^+[BF_4]^-$ and DBT are 1.824 Å (F3···H9), 2.549 Å (F2···H38), 2.311 Å (F2···H15), 2.381 Å (F1···H37), 2.463 Å (F1···H12), 2.960 Å (C25···H13), 3.329 Å (S21···H11), 3.466 Å (C33···C3), 3.596 Å (C29···N2), and 2.973 Å (C30···H16). The $[C_4mim]^+$ ring and DBT ring planes are parallel to each other, implying that π — π interactions may occur. The π stacking refers to attractive, non-covalent interactions between the aromatic rings.

The minimum energy geometries of $[C_6mim]^+[BF_4]^-$ are shown in Fig. 1, c. It can be seen that it has four F···H interactions, the corresponding interacting H15···F3, H17···F3, H9···F2, and H12···F1 distances being 2.882, 2.501, 1.795, and 2.153 Å. The shortest H9···F2 distance suggests that C1—H9 is involved in the formation of the strongest hydrogen bond. Hydrogen bonds also occur between the fluorine atoms of $[BF_4]^-$ and C—H of the methyl and ethyl groups (H15, H17, and H12) of the imidazolium ring. It can be seen that a single fluorine atom (F3) also participates in two hydrogen bonds. The most stable structure of $[C_6mim]^+[BF_4]^-$ —DBT is depicted in Fig. 2, c. In Fig. 2, c, the interacting

distances between $[C_6\text{mim}]^+[BF_4]^-$ and DBT are 2.024 Å (F1···H9), 2.305 Å (F1···H12), 2.066 Å (F3···H9), 2.272 Å (F3···H15), 2.293 Å (F2···H37), 2.315 Å (F2···H38), 2.959 Å (C25···H13), 3.551 Å (C27···N5), 3.786 Å (S21···C4), 3.556 Å (C33···C3), 3.616 Å (C29···N2), and 2.939 Å (C30···H16).

The optimized structure of $[C_8\text{mim}]^+[BF_4]^-$ (Fig. 1, d) shows the presence of four F···H interactions, the corresponding interacting H15···F3, H17···F3, H9···F2, and H12···F1 distances being 2.876, 2.488, 1.794, and 2.160 Å. The shortest H9···F2 distance suggests that C1—H9 is involved in the formation of the strongest hydrogen bond. Hydrogen bonds also occur between the fluorine atoms of $[BF_4]^-$ and C—H of the methyl and ethyl groups (H15, H17, and H12) of the imidazolium ring. A single fluorine atom (F3) also participates in two hydrogen bonds. The optimized interaction structure between $[C_8\text{mim}]^+[BF_4]^-$ and DBT shown in Fig. 2, d was obtained after screening many different potential arrangements. In Fig. 2, d, the interacting distances between $[C_8\text{mim}]^+[BF_4]^-$ and DBT are 1.975 Å (F1···H9), 2.406 Å (F1···H12), 2.122 Å (F3···H9), 2.202 Å (F3···H15), 2.295 Å (F2···H37), 2.313 Å (F2···H38), 2.982 Å (C25···H13), 3.551 Å (C27···N5), 3.794 Å (S21···C4), 3.578 Å (C33···C3), 3.606 Å (C29···N2), and 3.105 Å (C30···H16).

Among all the interactions between DBT and $[C_n\text{mim}]^+[BF_4]^-$, the calculated results show that H9 hydrogen bonds are the strongest ones, suggesting the crucial role of the C1 proton in the interaction between $[C_n\text{mim}]^+$ and $[BF_4]^-$ in terms of their short F···H distances, which is in agreement with the reported dominant role of C1 proton hydrogen bonds [28].

Interaction energies. The interaction energies are defined as differences between the sum of the DBT and $[C_2\text{mim}]^+[BF_4]^-/[C_4\text{mim}]^+[BF_4]^-/[C_6\text{mim}]^+[BF_4]^-/[C_8\text{mim}]^+[BF_4]^-$ energies and the energies of DBT — $[C_n\text{mim}]^+[BF_4]^-$ (with n: 2, 4, 6, 8) complexes.

The interaction energies of DBT- $[C_2\text{mim}]^+[BF_4]^-/[C_4\text{mim}]^+[BF_4]^-/[C_6\text{mim}]^+[BF_4]^-$ and $[C_8\text{mim}]^+[BF_4]^-$ complexes are collected in Table 1. This indicates the preferential adsorption of DBT by IL with a longer chain, which is in agreement with the experimental results of DBT extraction by $[C_n\text{mim}]^+[BF_4]^-$ [1]. The current results are consistent with the experimental results of Wilfred *et al.* [37].

AIM analysis. AIM theory can indicate the nature of interactions and the strength of hydrogen bonds through the electron density [17]. AIM theory has been used theoretically to a wide variety of structures containing different types of hydrogen interactions. These interactions can be successfully described by means of topological properties of the electron density distribution $\rho(r)$ using AIM2000. The electron density at BCP provides a measure of the strength of the bonding between two atoms. According to Bader's AIM theory [18], an atom, as defined by a space region delimited by its interatomic surfaces, is an accurate quantum open system. Hence, AIM can be used to examine the properties of atoms upon complexation. The AIM calculations show clearly the existence of BCP for each hydrogen bond in the complexes. The calculated values of the electron density $\rho(r)$ and the Laplacian of density $\nabla^2\rho(r)$ of dibenzothiophene, $[C_2\text{mim}]^+[BF_4]^-$ —DBT, $[C_4\text{mim}]^+[BF_4]^-$ —DBT, $[C_6\text{mim}]^+[BF_4]^-$ —DBT, and $[C_8\text{mim}]^+[BF_4]^-$ —DBT (a.u.) are collected in Table 2. This indicates the presence of remarkably strong interactions in the complexes. In all complexes the hydrogen bonds are typical of closed-shell interactions, as shown by positive values of the Laplacian of density $\nabla^2\rho(r)$. It has been noted that the electron densities $\rho(r)$ of hydrogen bonds with short distances are much greater than those of hydrogen bonds with long distances, which provides the preliminary evidence that the electron density is related to the hydrogen bond strength.

There are six BCPs between $[C_2\text{mim}]^+[BF_4]^-$ and DBT, seven BCPs between $[C_4\text{mim}]^+[BF_4]^-$ and DBT, eight BCPs between $[C_6\text{mim}]^+[BF_4]^-$ and DBT, eight BCPs between $[C_8\text{mim}]^+[BF_4]^-$ and DBT. The comparison of the ρ values for these BCPs can demonstrate the strong interaction in $[C_6\text{mim}]^+[BF_4]^-$ —DBT and $[C_8\text{mim}]^+[BF_4]^-$ —DBT.

NBO analysis. In order to investigate the present interactions in the studied target compounds, the NBO analysis of $[C_2\text{mim}]^+[BF_4]^-$, $[C_4\text{mim}]^+[BF_4]^-$, $[C_6\text{mim}]^+[BF_4]^-$, $[C_8\text{mim}]^+[BF_4]^-$, $[C_2\text{mim}]^+[BF_4]^-$ —DBT, $[C_4\text{mim}]^+[BF_4]^-$ —DBT, $[C_6\text{mim}]^+[BF_4]^-$ —DBT, and $[C_8\text{mim}]^+[BF_4]^-$ —DBT complexes was performed at the B3LYP/6-311++G(d,p) level. The NBO charges calculated by the natural population analysis (NPA) of the optimized structures of all compounds are given in Table 3.

Table 3

NBO charges on atoms for $[C_2\text{mim}]^+[BF_4]^-$, $[C_4\text{mim}]^+[BF_4]^-$, $[C_6\text{mim}]^+[BF_4]^-$, $[C_8\text{mim}]^+[BF_4]^-$, DBT— $[C_2\text{mim}]^+[BF_4]^-/[C_4\text{mim}]^+[BF_4]^-/[C_6\text{mim}]^+[BF_4]^-$ and $[C_8\text{mim}]^+[BF_4]^-$, obtained at the B3LYP/6-311G(d,p) level

Parameter	$[C_2\text{mim}]^+[BF_4]^-$	$[C_4\text{mim}]^+[BF_4]^-$	$[C_6\text{mim}]^+[BF_4]^-$	$[C_8\text{mim}]^+[BF_4]^-$	$[\text{Par}C_2\text{mim}]^+[BF_4]^-$ —DBT	$[C_4\text{mim}]^+[BF_4]^-$ —DBT	$[C_6\text{mim}]^+[BF_4]^-$ —DBT	$[C_8\text{mim}]^+[BF_4]^-$ —DBT	Parameter	$[\text{Par}C_2\text{mim}]^+[BF_4]^-$ —DBT	$[C_4\text{mim}]^+[BF_4]^-$ —DBT	$[C_6\text{mim}]^+[BF_4]^-$ —DBT	$[C_8\text{mim}]^+[BF_4]^-$ —DBT
C1	0.316	0.314	0.315	0.315	0.305	0.306	0.301	0.301	S21	0.374	0.374	0.373	0.373
N2	-0.359	-0.359	-0.360	-0.360	-0.364	-0.360	-0.358	-0.357	C22	-0.148	-0.149	-0.155	-0.155
C3	-0.024	-0.024	-0.025	-0.024	-0.015	-0.014	-0.015	-0.014	C23	-0.238	-0.239	-0.240	-0.241
C4	-0.024	-0.021	-0.020	-0.020	-0.024	-0.024	-0.021	-0.022	C24	-0.198	-0.198	-0.199	-0.199
N5	-0.360	-0.357	-0.357	-0.357	-0.357	-0.358	-0.357	-0.357	C24	-0.221	-0.221	-0.217	-0.217
C6	-0.364	-0.364	-0.364	-0.363	-0.362	-0.362	-0.367	-0.365	C26	-0.146	-0.145	-0.153	-0.152
C7	-0.167	-0.159	-0.159	-0.159	-0.185	-0.181	-0.180	-0.182	C27	-0.111	-0.112	-0.112	-0.112
C8	-0.590	-0.398	-0.395	-0.395	-0.583	-0.385	-0.381	-0.381	C28	-0.095	-0.095	-0.096	-0.096
H9	0.289	0.289	0.288	0.288	0.284	0.284	0.292	0.292	C29	-0.145	-0.145	-0.153	-0.153
H10	0.230	0.230	0.230	0.230	0.234	0.234	0.232	0.232	C30	-0.222	-0.223	-0.224	-0.224
H11	0.229	0.228	0.228	0.228	0.236	0.236	0.235	0.235	C31	-0.204	-0.204	-0.204	-0.204
H12	0.269	0.268	0.268	0.268	0.251	0.252	0.258	0.255	C32	-0.229	-0.230	-0.228	-0.228
H13	0.204	0.204	0.204	0.204	0.223	0.224	0.224	0.225	C33	-0.172	-0.173	-0.174	-0.174
H14	0.208	0.208	0.208	0.208	0.204	0.203	0.204	0.204	H34	0.214	0.214	0.214	0.214
H15	0.238	0.237	0.237	0.237	0.258	0.256	0.256	0.260	H35	0.209	0.209	0.209	0.209
H16	0.198	0.198	0.198	0.198	0.207	0.208	0.210	0.208	H36	0.215	0.215	0.215	0.215
H17	0.243	0.236	0.238	0.237	0.214	0.204	0.203	0.204	H37	0.241	0.244	0.253	0.253
H18	0.191	0.183	0.184	0.183	0.199	0.191	0.191	0.190	H38	0.241	0.243	0.252	0.252
B	1.343	1.343	1.343	1.343	1.342	1.342	1.347	1.348	H39	0.216	0.216	0.214	0.214
F1	-0.584	-0.584	-0.584	-0.584	-0.588	-0.588	-0.591	-0.590	H40	0.208	0.207	0.207	0.207
F2	-0.581	-0.581	-0.581	-0.580	-0.583	-0.585	-0.570	-0.570	H41	0.214	0.213	0.212	0.213
F3	-0.583	-0.582	-0.583	-0.583	-0.576	-0.575	-0.592	-0.593					
F4	-0.541	-0.542	-0.542	-0.542	-0.542	-0.542	-0.544	-0.544					

It is clear that DBT adsorption on $[C_2\text{mim}]^+[BF_4]^-/[C_4\text{mim}]^+[BF_4]^-/[C_6\text{mim}]^+[BF_4]^-/[C_8\text{mim}]^+[BF_4]^-$ ILs influences their charges distributions. As compared with the NBO charges, the hydrogen atoms involved in hydrogen bonds are more positive. The results indicate that the H9 atom carries the most positive charge as compared to the other hydrogen atoms for all compounds. Nowadays, it seems quite well accepted that the hydrogen bonding influences the IL structures. The aim of this section is to discern the extent of hydrogen bonding contacts using the NBO analysis results.

Table 4 lists the donor-acceptor NBO interactions and their $E(2)$ values in $[C_2\text{mim}]^+[BF_4]^-$, $[C_4\text{mim}]^+[BF_4]^-$, $[C_6\text{mim}]^+[BF_4]^-$, $[C_8\text{mim}]^+[BF_4]^-$, $[C_2\text{mim}]^+[BF_4]$ —DBT, $[C_4\text{mim}]^+[BF_4]$ —DBT, $[C_6\text{mim}]^+[BF_4]$ —DBT, and $[C_8\text{mim}]^+[BF_4]$ —DBT.

The extent of electron delocalization from donors to acceptors can be evaluated by analyzing the second order perturbation stabilization energy $E(2)$, which indicates the intensity of interactions between the orbitals of electron donors and acceptors. The higher the $E(2)$ value, the more the electrons are transferred from donor orbitals to acceptor orbitals.

Table 4

*Selected second order energy analyses for NBO interactions ($E^{(2)}$, kcal/mol) in the studied compounds, obtained at the B3LYP/6-311G(*d,p*) level*

Parameter	[C ₂ mim] ⁺ [BF ₄] ⁻	[C ₄ mim] ⁺ [BF ₄] ⁻	[C ₆ mim] ⁺ [BF ₄] ⁻	[C ₈ mim] ⁺ [BF ₄] ⁻	[C ₂ mim] ⁺ [BF ₄] ⁻ —DBT	[C ₄ mim] ⁺ [BF ₄] ⁻ —DBT	[C ₆ mim] ⁺ [BF ₄] ⁻ —DBT	[C ₈ mim] ⁺ [BF ₄] ⁻ —DBT
LP _(F1) → σ _(C1—H9) [*]	—	—	—	—	0.09	0.06	5.43	6.96
LP _(F1) → σ _(C6—H12) [*]	2.80	2.81	2.77	2.68	0.71	0.74	1.55	1.06
LP _(F1) → σ _(C6—H13) [*]	0.07	0.06	0.06	0.06	—	—	—	—
LP _(F1) → σ _(C6—H14) [*]	—	—	—	—	—	0.06	—	—
LP _(F1) → σ _(C26—H37) [*]	—	—	—	—	0.53	0.75	—	—
LP _(F2) → σ _(C1—H9) [*]	15.40	15.30	15.20	15.30	—	—	—	—
LP _(F2) → σ _(C7—H15) [*]	—	—	—	—	2.04	1.75	—	—
LP _(F2) → σ _(C26—H37) [*]	—	—	—	—	—	—	2.07	2.04
LP _(F2) → σ _(C29—H38) [*]	—	—	—	—	0.36	0.43	1.92	1.93
LP _(F3) → σ _(C7—H15) [*]	0.08	0.08	0.08	0.09	—	—	1.69	2.19
LP _(F3) → σ _(C1—H9) [*]	—	—	—	—	15.11	14.24	4.15	3.15
LP _(F3) → σ _(C7—H16) [*]	0.09	0.09	0.09	0.10	—	—	—	—
LP _(F3) → σ _(C8—H17) [*]	0.30	0.44	0.46	0.49	—	—	—	—
LP _(F4) → σ _(C1—H9) [*]					—	0.18	0.06	0.07
LP _(S21) → σ _(C4—H11) [*]					0.12	0.12	0.09	0.05
π _(C1—N5) → π _(C22—C27) [*]					—	—	0.08	0.07
π _(C3—C4) → π _(C28—C29) [*]					0.13	0.14	0.06	0.05
π _(C3—C4) → π _(C32—C33) [*]					0.1	0.12	0.11	0.1
π _(C22—C27) → π _(C1—N5) [*]					—	—	0.06	0.06
π _(C22—C27) → π _(C3—C4) [*]					0.32	0.32	0.16	0.13
π _(C22—C27) → σ _(C6—H13) [*]					—	—	0.06	0.07
π _(C23—C24) → σ _(C6—H13) [*]					0.13	0.13	0.27	0.33
π _(C25—C26) → σ _(C6—H13) [*]					0.12	0.14	0.06	—
π _(C25—C26) → σ _(C6—H14) [*]					0.06	0.06	0.06	0.06
π _(C28—C29) → π _(C1—N5) [*]					0.05	0.07	0.24	0.25
π _(C30—C31) → σ _(C7—H16) [*]					0.21	0.34	0.41	0.39
π _(C32—C33) → π _(C3—C4) [*]					0.14	0.17	0.17	0.15

Inspection of Table 4 shows that there is a strong hydrogen bonding interaction between F2 and H9 in $[C_2\text{mim}]^+[BF_4]^-$, $[C_4\text{mim}]^+[BF_4]^-$, $[C_6\text{mim}]^+[BF_4]^-$, $[C_8\text{mim}]^+[BF_4]^-$, and its second order interaction energy $LP_{(F2)} \rightarrow \sigma_{(C1-H9)}^*$ are 15.40, 15.30, 15.20, 15.30 kcal/mol⁻¹, respectively. The large second order perturbation stabilization energies of 15.11 kcal/mol⁻¹ in $[C_2\text{mim}]^+[BF_4]^-$ —DBT and 14.24 kcal/mol⁻¹ in $[C_4\text{mim}]^+[BF_4]^-$ —DBT indicate the strong hydrogen bonding between F3 and H9 atoms.

The larger summation of second order perturbation stabilization energies of $LP_{(F2)} \rightarrow \sigma_{(C26-H37)}^*$, $LP_{(F2)} \rightarrow \sigma_{(C29-H38)}^*$, $LP_{(S21)} \rightarrow \sigma_{(C4-H11)}^*$, $\pi_{(C1-N5)} \rightarrow \pi_{(C22-C27)}^*$, $\pi_{(C3-C4)} \rightarrow \pi_{(C28-C29)}^*$, $\pi_{(C3-C4)} \rightarrow \pi_{(C32-C33)}^*$, $\pi_{(C22-C27)} \rightarrow \pi_{(C1-N5)}^*$, $\pi_{(C22-C27)} \rightarrow \pi_{(C3-C4)}^*$, $\pi_{(C22-C27)} \rightarrow \sigma_{(C6-H13)}^*$, $\pi_{(C23-C24)} \rightarrow \sigma_{(C6-H13)}^*$, $\pi_{(C25-C26)} \rightarrow \sigma_{(C6-H13)}^*$, $\pi_{(C25-C26)} \rightarrow \sigma_{(C6-H14)}^*$, $\pi_{(C28-C29)} \rightarrow \pi_{(C1-N5)}^*$, $\pi_{(C30-C31)} \rightarrow \sigma_{(C7-H16)}^*$, $\pi_{(C32-C33)} \rightarrow \pi_{(C3-C4)}^*$ between $[C_6\text{mim}]^+[BF_4]^-$ and DBT, and $[C_8\text{mim}]^+[BF_4]^-$ and DBT than $LP_{(F1)} \rightarrow \sigma_{(C26-H37)}^*$, $LP_{(F2)} \rightarrow \sigma_{(C29-H38)}^*$, $LP_{(S21)} \rightarrow \sigma_{(C4-H11)}^*$, $\pi_{(C3-C4)} \rightarrow \pi_{(C28-C29)}^*$, $\pi_{(C3-C4)} \rightarrow \pi_{(C32-C33)}^*$, $\pi_{(C22-C27)} \rightarrow \pi_{(C3-C4)}^*$, $\pi_{(C23-C24)} \rightarrow \sigma_{(C4-H11)}^*$, $\pi_{(C25-C26)} \rightarrow \sigma_{(C6-H13)}^*$, $\pi_{(C25-C26)} \rightarrow \sigma_{(C6-H14)}^*$, $\pi_{(C28-C29)} \rightarrow \pi_{(C1-N5)}^*$, $\pi_{(C30-C31)} \rightarrow \sigma_{(C7-H16)}^*$, $\pi_{(C32-C33)} \rightarrow \pi_{(C3-C4)}^*$ between $[C_2\text{mim}]^+[BF_4]^-$ and DBT, and $[C_4\text{mim}]^+[BF_4]^-$ and DBT might be caused by the more effective interaction in $[C_6\text{mim}]^+[BF_4]^-$ —DBT and $[C_8\text{mim}]^+[BF_4]^-$ —DBT.

CONCLUSIONS

The interaction energies of DBT and $[C_2\text{mim}]^+[BF_4]^-/[C_4\text{mim}]^+[BF_4]^-/[C_6\text{mim}]^+[BF_4]^-/[C_8\text{mim}]^+\times[BF_4]^-$ complexes have been calculated at the B3LYP/6-311++G** level using the DFT method. The most stable optimized structures of $[C_2\text{mim}]^+[BF_4]^-$ —DBT, $[C_4\text{mim}]^+[BF_4]^-$ —DBT, $[C_6\text{mim}]^+[BF_4]^-$ —DBT, and $[C_8\text{mim}]^+[BF_4]^-$ —DBT were obtained by NBO and AIM analyses. The optimized structures suggest that the DBT rings are parallel to the rings of the imidazolium cations, indicating the occurrence of $\pi-\pi$ interactions as corroborated by NBO and AIM analyses.

The calculated results show that the interaction energies of DBT and $[C_n\text{mim}]^+[BF_4]^-$ have higher values with larger alkyl chain lengths. Generally, it seems that $[R\text{mim}]^+[BF_4]^-$ ILs with longer alkyl chains is an appropriate option for extractive desulfurization. The above results may help us to design extractants and improve the operating conditions.

REFERENCES

1. Zhang S., Zhang Q., Zhang Z.C. // Industrial & Engineer. Chem. Res. – 2003. – **43**. – P. 614 – 622.
2. Gao J.-J., Li H.-Q., Zhang H.-X. et al. // Industrial & Engineer. Chem. Res. – 2012. – **51**. – P. 4682 – 4691.
3. Alonso L., Arce A., Francisco M. et al. // Fluid Phase Equilibria. – 2008. – **270**. – P. 97 – 102.
4. Stanislaus A., Marafi A., Rana M.S. // Catalysis Today. – 2010. – **153**. – P. 1 – 68.
5. Anantharaj R., Banerjee T. // Fluid Phase Equilibria. – 2010. – **293**. – P. 22 – 31.
6. Rodríguez-Cabo B., Soto A., Arce A. // J. Chem. Thermodyn. – 2013. – **57**. – P. 248 – 255.
7. Akbari A., Omidkhah M., Darian J.T. // Ultrasonics Sonochemistry. – 2014. – **21**. – P. 692 – 705.
8. Nie Y., Li C., Meng H. et al. // Fuel Processing Technology. – 2008. – **89**. – P. 978 – 983.
9. Alonso L., Arce A., Francisco M. et al. // Fluid Phase Equilibria. – 2008. – **270**. – P. 97 – 102.
10. Zhou J., Mao J., Zhang S. // Fuel Processing Technology. – 2008. – **89**. – P. 1456 – 1460.
11. Velu S., Ma X., Song C. // Industrial & Engineer. Chem. Res. – 2003. – **42**. – P. 5293 – 5304.
12. Li H., He L., Lu J. et al. // Energy & Fuels. – 2009. – **23**. – P. 1354 – 1357.
13. Vakili-Nezhaad G., Vatani M., Asghari M. et al. // J. Chem. Thermodyn. – 2012. – **54**. – P. 148 – 154.
14. Vraneš M.B., Dožić S., Djerić V. et al. // J. Chemical & Engineer. Data. – 2013. – **58**. – P. 1092 – 1102.
15. Shekaari H., Bezaatpour A., Elhami-Kalvanagh R. // J. Chem. & Engineer. Data. – 2012. – **57**. – P. 345 – 351.
16. Chandra Srivastava V. // RSC Advances. – 2012. – **2**. – P. 759 – 783.
17. Lü R., Qu Z., Lin J. // J. Mol. Liq. – 2013. – **180**. – P. 207 – 214.
18. Lü R., Lin J., Qu Z. // Comput. Theor. Chem. – 2012. – **1002**. – P. 49 – 58.

19. Kędra-Krolik K., Mutelet F., Moïe J.-C. et al. // Energy & Fuels. – 2011. – **25**. – P. 1559 – 1565.
20. Alonso L., Arce A., Francisco M. et al. // J. Chem. Thermodyn. – 2008. – **40**. – P. 966 – 972.
21. Francisco M., Arce A., Soto A. // Fluid Phase Equilibria. – 2010. – **294**. – P. 39 – 48.
22. Revelli A.-L., Mutelet F., Jaubert J.-N.L. // J. Phys. Chem. B. – 2010. – **114**. – P. 4600 – 4608.
23. Potdar S., Anantharaj R., Banerjee T. // J. Chem. & Engineer. Data. – 2012. – **57**. – P. 1026 – 1035.
24. Kędra-Królik K., Fabrice M., Jaubert J.-N.L. // Industrial & Engineer. Chem. Res. – 2011. – **50**. – P. 2296 – 2306.
25. Anantharaj R., Banerjee T. // J. Chem. & Engineer. Data. – 2011. – **56**. – P. 2770 – 2785.
26. Batista M.L.S., Tomé L.I.N., Neves C.M.S.S. et al. // J. Phys. Chem. B. – 2012. – **116**. – P. 5985 – 5992.
27. Liu X., Zhou G., Zhang X. et al. // AIChE Journal. – 2010. – **56**. – P. 2983 – 2996.
28. Xu D., Zhu W., Li H. et al. // Energy & Fuels. – 2009. – **23**. – P. 5929 – 5933.
29. Frisch M.J., Trucks G.W., Schlegel H.B. et al. // Gaussian 03, Revision B.03, Gaussian, Inc., Pittsburgh PA, 2003.
30. Becke A.D. // J. Chem. Phys. – 1993. – **98**. – P. 5648 – 5652.
31. Lee C., Yang W., Parr R.G. // Phys. Rev. B. – 1988. – **37**. – P. 785 – 789.
32. Reed A.E., Curtiss L.A., Weinhold F. // Chem. Rev. – 1988. – **88**. – P. 899 – 926.
33. Glendening E.D., Reed A.E., Carpenter J.E. et al. // NBO Version 3.1.
34. Bader R.F.W. Atoms in molecules. A quantum theory. – Oxford, UK: Clarendon Press, 1990.
35. Biegler Konig F.W., Schonbohm J., Bayles D. // J. Comput. Chem. – 2001. – **22**. – P. 545 – 559.
36. Lü R., Qu Z., Yu H. et al. // Comput. Theor. Chem. – 2012. – **988**. – P. 86 – 91.
37. Wilfred C.D., Kiat C.F., Man Z. et al. // Fuel Processing Technology. – 2012. – **93**. – P. 85 – 89.